Molecular Crystals and Liquid Crystals

Publication details, including instructions for authors and subscription information:
http://www.tandfonline.com/loi/gmcl20

Effects of Dielectric Relaxation on the Dynamics and Dielectric Heating of Nematic Liquid Crystals

Sergij V. Shiyanovskii [a], Andrii B. Golovin [a], Ye Yin [a] & Oleg D. Lavrentovich [a]

[a] Liquid Crystal Institute and Chemical Physics Interdisciplinary Program, Kent State University, Kent, OH

Version of record first published: 22 Sep 2010

To cite this article: Sergij V. Shiyanovskii, Andrii B. Golovin, Ye Yin & Oleg D. Lavrentovich (2008): Effects of Dielectric Relaxation on the Dynamics and Dielectric Heating of Nematic Liquid Crystals, Molecular Crystals and Liquid Crystals, 480:1, 111-128

To link to this article: http://dx.doi.org/10.1080/15421400701825805

Mol. Cryst. Liq. Cryst., Vol. 480, pp. 111–128, 2008

ISSN: 1542-1406 print/1563-5287 online
DOI: 10.1080/15421400701825805

Taylor & Francis
Taylor & Francis Group

Effects of Dielectric Relaxation on the Dynamics and Dielectric Heating of Nematic Liquid Crystals

Sergij V. Shiyanovskii, Andrii B. Golovin, Ye Yin, Oleg D. Lavrentovich
Liquid Crystal Institute and Chemical Physics Interdisciplinary Program, Kent State University, Kent, OH

We present recent experimental and theoretical results that link the phenomenon of dielectric relaxation in nematic liquid crystals to their fast electro-optical switching and to the problem of dielectric heating. We develop the theoretical model that allows one to relate director reorientation to the "history" of the electric field. We present an experiment that is well described by the proposed theory but which cannot be described within the classic model of an instantaneous response. We also analyze the effect of dielectric heating that is especially profound at the frequencies corresponding to dielectric relaxation.

Keywords: dielectric heating; dielectric relaxation; dielectric torque; dual frequency nematic liquid crystals; orientational dynamics

1. INTRODUCTION

Orientational dynamics of nematic liquid crystals (NLCs) in the electric field caused by dielectric anisotropy of these materials is a fundamental physical phenomenon that is at the heart of numerous modern technologies. The director $\mathbf{n}$ that is the direction of the average molecular orientation and simultaneously the optic axis of the NLC, reorients under the action of the dielectric torque of density $\mathbf{M}(t) = \mathbf{D}(t) \times \mathbf{E}(t)$, where $\mathbf{E}(t)$ is the electric field and $\mathbf{D}(t)$ is the electric

We acknowledge the support of NSF Grants DMR 0315523 and 0504516 and DOE grant DE-FG02-06ER 46331; Y. Y. acknowledges the support of Samsung Electronics Corporation through the Samsung Scholarship at the Liquid Crystal Institute/Chemical Physics Interdisciplinary Program, KSU; we thank O.P. Pishnyak for the measurements of refractive indices.

Address correspondence to Sergij V. Shiyanovskii, Liquid Crystal Institute and Chemical Physics Interdisciplinary Program, Kent State University, Kent, Ohio 44242, USA. E-mail: svshiyan@lci.kent.edu

displacement at the moment of time t. The finite rate of dielectric relaxation causes a time lag of the electric displacement as compared to the instantaneous value of the electric field. This previously ignored effect is the subject of our study. We show that it causes profound effects when the characteristic times of the field and director changes are close to the dielectric relaxation time. Depending on the type of the nematic material, the characteristic relaxation times range from milliseconds (dual-frequency materials) to nanoseconds ("regular" materials such as pentylcyanobiphenyl). From the fundamental viewpoint, the problem is to determine the dielectric torque as a function of not only the present values of the electric field and director (as in the current theory) but of the previous values of these variables. Nematic devices are capable of switching in nanosecond [1] and microsecond [2] ranges, thus the issue of finite rate of dielectric relaxation is also of practical importance.

In this article, we propose a general model to describe the time-dependent dielectric response of NLCs. The corresponding theories exist for isotropic fluids and solid crystals: in both cases, the dielectric properties of the medium do not change with time [3]. In the NLC, however, the situation is more complex, as the electric field causes director reorientation which in its turn changes the dielectric coupling between the field and the medium. We present an experiment that is well described by the proposed theory but which cannot be described within the classic model of an instantaneous response [4]. The next section describes the basic experimental setup that allows one to achieve a fast switching, followed by the theory and then by verification of the theory and the experiment. We also investigate the other processes that occur during the fast switching, namely slow relaxation and dielectric heating.

2. FAST SWITCHING: EXPERIMENT

We use the so-called dual-frequency nematic materials [5] in antiparallel cells with a high pretilt angle ($\alpha \approx 30$–70, preferably close to 40–50 degrees) driven by a sequence of electric pulses of different frequency and amplitude. The high pretilt angle is achieved by an oblique deposition of SiO layers (Fig. 1), although some polyimides can be used, as well. High value of the pretilt angle has several advantages. First, the dielectric torque of the applied field, which scales as $\sim \sin\theta\cos\theta \sim \sin 2\theta$, is maximized when the angle θ between the director and the field is about 45 degrees, so that $\sin 2\theta \approx 1$. Second, there is no threshold for director reorientation. Third, high pretilt

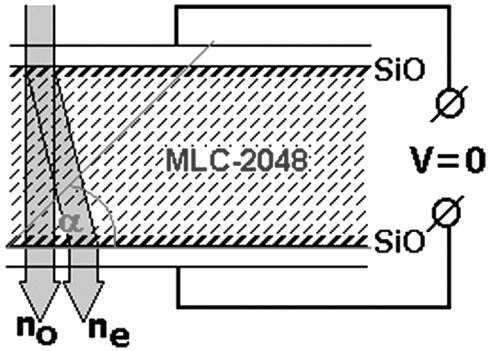

FIGURE 1 Initial tilted orientation of dual frequency nematic cell.

guaranties strong restoring surface torques that facilitates reorientation from both the homeotropic and the planar states.

Depending on the frequency of the applied voltage, the director reorients towards homeotropic state or towards the planar state (Fig. 1), because the dielectric anisotropy $\Delta\varepsilon$ of the dual-frequency nematic changes the sign at crossover frequency. For example, in our nematic material MLC-2048 $\Delta\varepsilon = 3.22$ at 1 kHz and $\Delta\varepsilon = -3.5$ at 100 kHz at the room temperature.

The speed of switching of the cell can be determined by measuring the intensity of He–Ne laser light ($\lambda = 633$ nm) passing through the cell; the light is linearly polarized under the angle 45 degrees with respect to the "easy" axes direction in the plane of the cell. The intensity is determined as $I(\Delta\varphi) = I_0 \sin^2(\Delta\varphi/2)$, where I_0 is the intensity of incident light (we neglect small corrections due to the reflection of light at interfaces, scattering at director fluctuations, etc.) and $\Delta\varphi$ is the phase shift acquired by the light passing through the cell:

$$\Delta\varphi = \frac{2\pi n_o}{\lambda} \int_0^d \left(\frac{n_e}{\sqrt{n_o^2 \sin^2\theta(z,t) + n_e^2 \cos^2\theta(z,t)}} - 1 \right) dz \qquad (1)$$

In MLC-2048 the extraordinary and ordinary indices of refraction are $n_e = 1.705$ and $n_o = 1.495$ at $\lambda = 633$ nm.

The dual-frequency nematic allows us to control the switching dynamics in both directions by the applied voltage. Figure 2 shows the transmitted intensity (top trace) versus the applied voltage (bottom trace) at two frequencies (50 kHz and 1 kHz) when the voltage applied to a hybrid aligned nematic cell varies slowly with the rate 2.5 V/s. For such a slow rate, the dielectric behavior can be regarded

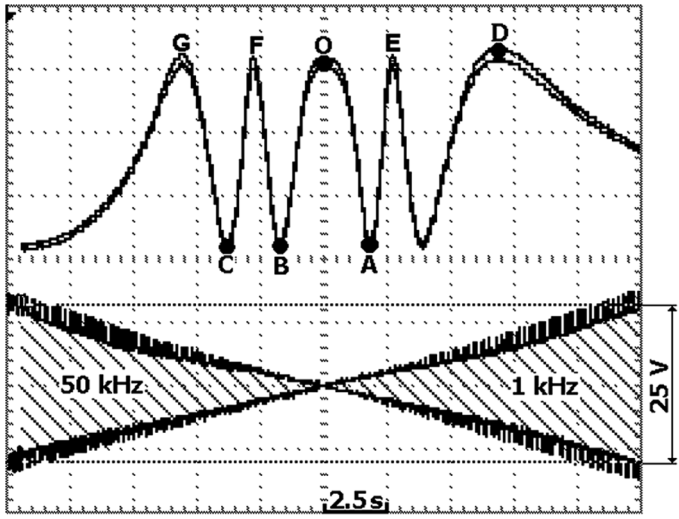

FIGURE 2 Optical transmission of 14.5 μm thick nematic cell (top trace) registered by the photodetector as the function of applied voltage (bottom trace shows envelop of the voltage waveform) at 50 kHz (left part) and 1 kHz (right part).

as a quasi-static dielectric response, where the standard description with an instantaneous relation between the displacement and the field is valid. We start with the special short pulse (SSP) of large amplitude to speed up the switching. The low- and high-frequency SSPs are used

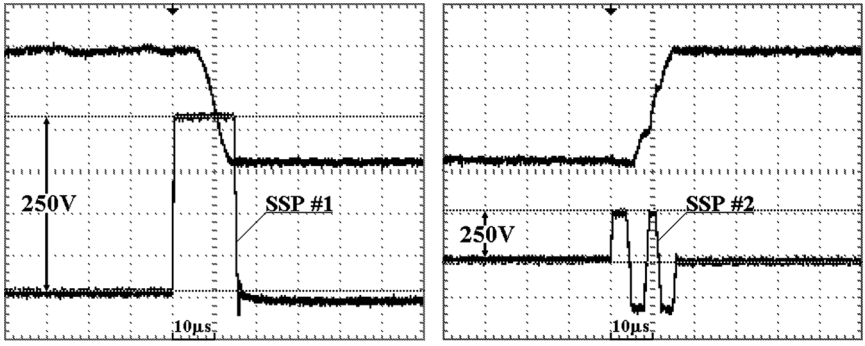

FIGURE 3 Fast switching of phase shift $\Delta L \approx 0.3\mu$m by (a) square pulse; (b) high frequency pulse. The top trace shows the light intensity change and the bottom shows the voltage profile.

for switching toward the homeotropic and planar states, respectively [2]. Amplitude and duration of the SSP were adjusted to minimize the transition time to the final state, which is controlled by the following "holding" voltage of appropriate frequency and amplitude. The scheme allows us to achieve 2 μm optical retardation shift during 0.4 ms; 0.3 μm switches can be achieved much faster, approximately within 15 μs.

An example of the applied voltage profile with two SSPs is presented in Figure 3. The first square SSP (duration 15 μs) produces fast reorientation of phase shift $\Delta L \approx 0.3\,\mu\text{m}$. Figure 2(b) shows how the cell is switched back to the original state; we used the second SSP (duration 16 μs, frequency 125 kHz).

3. DIELECTRIC DISPERSION AND DIELECTRIC TORQUE: THEORY [7]

The superposition rule in the classical electromagnetic theory results in the following dependence:

$$\mathbf{D}(t) = \varepsilon_0 \mathbf{E}(t) + \varepsilon_0 \int_{-\infty}^{t} \alpha(t,t')\mathbf{E}(t')du \tag{2}$$

where $\alpha(t,t')$ is the step response tensor describing the contribution of the electric field at the moment $t' \le t$. To analyze the dynamics, it is useful to split $\alpha(t,t')$ into a fast $\alpha_f(t,t')$ and a slow $\alpha_s(t,t')$ contributions with respect to the director rotation and to the rate of electric field change, $\alpha(t,t') = \alpha_f(t,t') + \alpha_s(t,t')$, so that Eq. (2) reads

$$\mathbf{D}(t) = \varepsilon_0 \varepsilon_f(t)\mathbf{E}(t) + \varepsilon_0 \int_{-\infty}^{t} \alpha_s(t,\, t')\mathbf{E}(t')dt', \tag{3}$$

The slow part $\alpha_s(t,t')$ is caused by reorientation of the permanent molecular dipoles in the NLC. Even when the director angular velocity is high and approaches the relaxation rate of polarization, the director-imposed slow rotation of all molecules should not affect substantially the fast individual flip-flops responsible for the dielectric relaxation. The latter assumption implies that $\alpha_s(t,t')$ can be expressed through the step response tensor component $\alpha_{||}(t-t')$ along the director, when the director is fixed:

$$\alpha_s(t,t') = \alpha_{||}(t-t')\hat{\mathbf{n}}(t) \otimes \hat{\mathbf{n}}(t'). \tag{4}$$

Here $\otimes$ stands for the external product of two vectors, which is the tensor with the components $[\hat{\mathbf{n}}(t) \otimes \hat{\mathbf{n}}(t)]_{ij} = n_i(t)n_j(t)$. The classical

Debye's theory of relaxation predicts an exponential decay of $\alpha_{\|}(t-t')$ and a Lorenzian behavior for $\varepsilon_{\|}(\omega)$ [6,7].

$$\alpha_{\|}(t-t') = \frac{\varepsilon_{l\|} - \varepsilon_{h\|}}{\tau_{\|}} \exp\left(-\frac{t-t'}{\tau_{\|}}\right), \quad \varepsilon_{\|}(\omega) = \frac{\varepsilon_{l\|} - \varepsilon_{h\|}}{1 - i\omega\tau_{\|}} \tag{5}$$

where $\varepsilon_{l\|}$ and $\varepsilon_{h\|}$ are $\varepsilon_{\|}(\omega)$ at low and high frequencies, respectively. In this case the resulting dielectric torque density for the uniaxial NLC is:

$$\mathbf{M}(t) = \varepsilon_0 \hat{\mathbf{n}}(t) \times \mathbf{E}(t) \left\{ (\varepsilon_{h\|} - \varepsilon_{\square}) \hat{\mathbf{n}}(t) \cdot \mathbf{E}(t) + \frac{\varepsilon_{l\|} - \varepsilon_{h\|}}{\tau_{\|}} \int_{-\infty}^{t} \exp\left(-\frac{t-t'}{\tau_{\|}}\right) \hat{\mathbf{n}}(t') \cdot \mathbf{E}(t') dt' \right\}. \tag{6}$$

The dielectric memory effect is described by the integral term of Eq. (6), which is absent in the standard approach.

4. DIELECTRIC DISPERSION AND DIELECTRIC TORQUE: EXPERIMENT VS. THEORY [4]

To test the competition between the instantaneous and memory contributions to the total torque, Eq. (6), we traced the director dynamics by measuring the optical phase retardation of the DFN cell, Figure 4, where the light intensity that corresponds to the zero-field point O is in the center of the entire range. The dielectric memory effect described by the last term in Eq. (6) becomes evident when the voltage changes abruptly. The behavior of light intensity recorded for 100 kHz pulses in Figure 5(a) is in agreement with the quasi-static behavior in Figure 4. However, the initial response to a step-like pulse of a low frequency, Figure 5(b), is exactly opposite to what is expected from the quasi-static model and experiment in Figure 4. Namely, Figure 4 suggests that the light intensity should increase towards point A when the voltage is increased at 1 kHz, while Figure 5(b) demonstrates that the voltage pulse actually decreases the light intensity (towards point Y in Fig. 5(b)) at the beginning of director reorientation. This anomalous decrease is not related to the possible parasitic effects such as light scattering losses: The insert in Figure 5(b) demonstrates that the trend is reversed when an additional π phase retarder (Soleil-Babinet compensator SB-10 purchased from Optics for Research) is inserted between the cell and the polarizer. Therefore, the reason for the different response of the director to the quasi-static, Figure 4, and abrupt, Figure 5(b), voltage increase at 1 kHz is not related to the parasitic

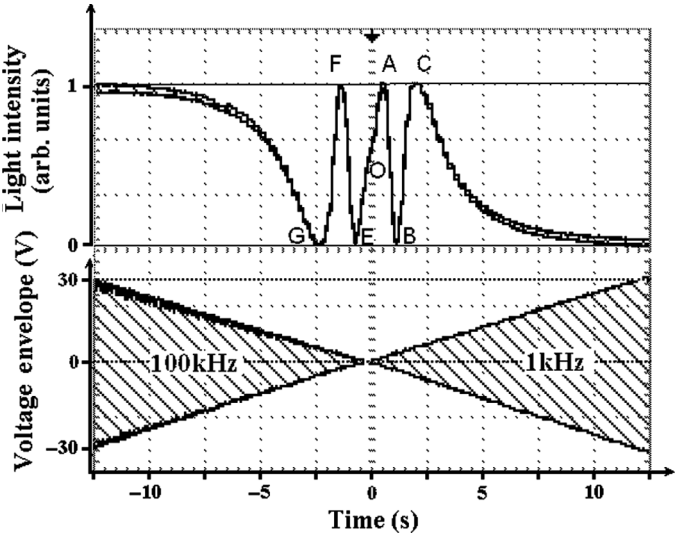

FIGURE 4 Transmitted light intensity modulated by the changes of optical retardation (the top curve) vs. slowly changing sinusoidal voltage (the bottom trace that shows the envelope of sinusoidal signal) applied at two different frequencies 100 kHz (left part) and 1 kHz (right part) to the MLC2048 cell of thickness $d = 10\,\mu\text{m}$. Point O corresponds to light transmittance at zero voltage; points A, B, etc. are the extrema of the light intensity curve where $\Delta\varphi = k\pi$; k is an integer.

effects and might be caused by the dielectric memory effect, i.e., by the fact that $\mathbf{D}(t) \neq \varepsilon_0\varepsilon\mathbf{E}(t)$.

To verify this hypothesis, we simulated the transmitted light intensity using Eq. (6). The polar angle $\theta(z,t)$ between $\hat{\mathbf{n}}$ and the normal to the cell is described by the Erickson-Leslie equation; we neglected the backflow effects as we are interested in the very beginning of field-induced reorientation; the initial condition is $\theta(z, t = 0) = \theta_0 = 45^\circ$ at $M(t < 0) = 0$. We independently measured the rotation viscosity $\gamma = 0.3\,\text{kg} \cdot \text{m}^{-1} \cdot \text{s}^{-1}$ [8], and the elastic constants $K_1 = 17.7$ pN and $K_3 = 21.4$ pN, the cell thickness $d = 10\,\mu\text{m}$; the extraordinary and ordinary indices of refraction: $n_e = 1.705$ and $n_o = 1.495$ (both at $\lambda = 633\,\text{nm}$). The experimental light intensity curves in Figure 5 are compared to the two models: the model developed in this work, Eq. (6) (dashed lines), and the standard model (dotted line) with an instantaneous relationship $\mathbf{D}(t) = \varepsilon_0\varepsilon\mathbf{E}(t)$. The new model agrees well with the experiment, while the standard model contradicts it. The standard model, as compared to the experiment, shows the opposite

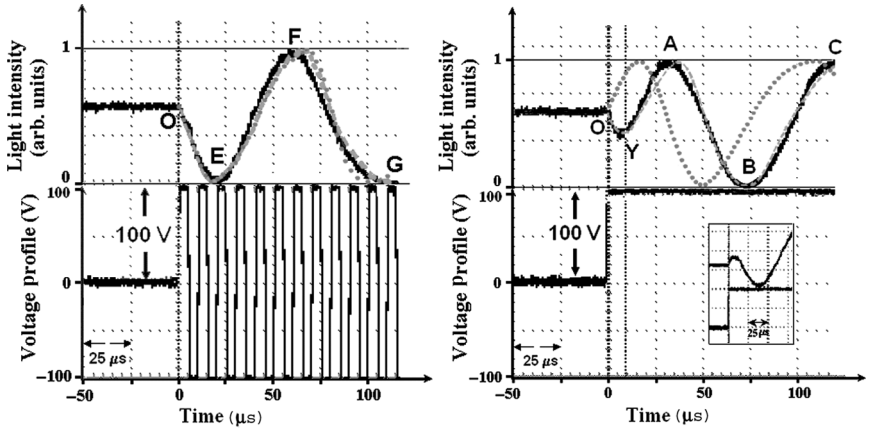

FIGURE 5 Transmitted light intensity modulated by the changes of optical retardation for the same DFN cell as in Figure 4, but driven by steep changes of the applied voltage at 100 kHz (a) and 1 kHz (b). The voltage profile is shown by the lower traces. The time scale is 25 μs/sqr. In the top parts, the solid lines are the oscilloscope's trace for the experimentally determined light transmittance, the dashed lines represent the transmitted intensity as calculated from our model (6), and the dotted lines represent the standard approach with $\mathbf{D}(t) = \varepsilon_0 \varepsilon \mathbf{E}(t)$. Point "Y" corresponds to the maximum director reorientation in the "wrong" direction. The insert is the optical transmission for the DFN cell driven by a 1 kHz pulse when a π phase retarder is inserted between the polarizer and the cell.

direction of intensity changes and thus the opposite direction of the director reorientation when the amplitude of 1 kHz voltage changes abruptly, Figure 5(b).

5. SLOW RELAXATION AFTER THE FAST SWITCHING

In this article we study the possibility of slow relaxation after the fast switching caused by SSP pulse. Two mechanisms may contribute to such relaxation: (a) back-flow effects and (b) director reorientation caused by the difference between $\theta(z,t)$ after SSP pulse and the equilibrium $\theta_{eq}(z)$ that corresponds to the applied holding voltage after the SSP pulse. We investigate the dynamics of the transitions between the states shown in Figure 2, that correspond to the extrema of the retardation signal. The amplitude and duration of SSP were adjusted to minimize slow relaxation. The transitions with a step of $\Delta\varphi = \pi$ from initial state O toward the planar state are shown in Figure 6. For

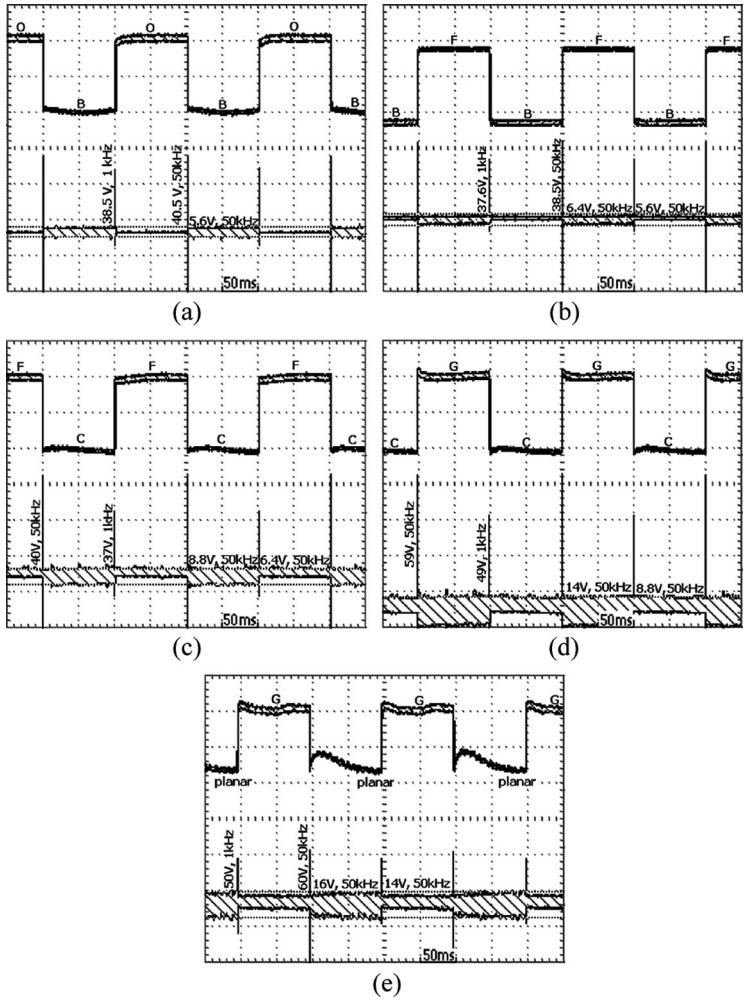

FIGURE 6 Fast optical retardation switching by steps between states O, B, F, C, G and planar shown in Figure 2.

the first four steps exhibit we effectively suppressed the relaxation effects. Only for the last step #5, the director reorientation remained substantial with whole range of adjusting parameters. We attribute it to the fact that this transition is between highly distorted quasi planar states and requires big director deformation.

We observed that for the transition toward the homeotropic state even by larger step of 4π from O to D state in Figure 2, produces

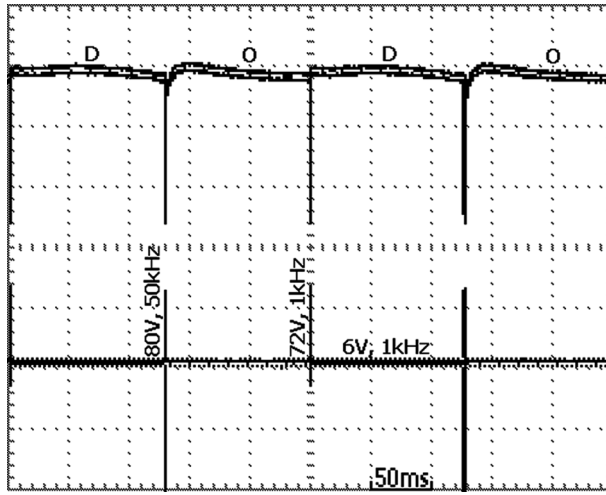

FIGURE 7 Fast optical retardation switching between states O and D shown in Figure 2.

relatively small relaxation effects, Figure 7. The larger relaxation effects for the D to O transition in the opposite direction are probably caused by back-flow effect. This asymmetry in relaxation becomes tremendous for a hybrid cell, Figure 8.

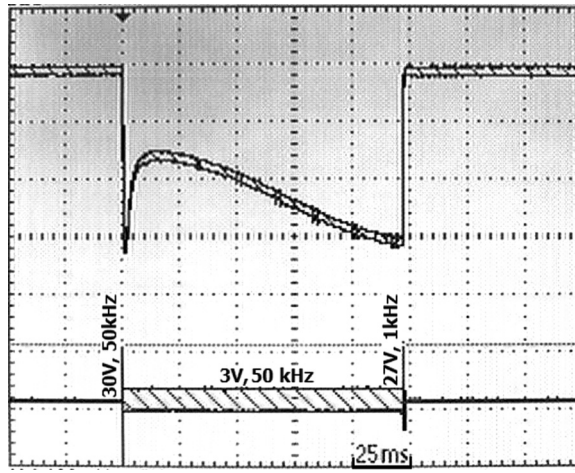

FIGURE 8 Fast switching of optical retardation on $\Delta\varphi = \pi$ by using cell of the hybrid alignment.

We think that further suppression of slow relaxation can achieved by modifying the shape of the SSP pulse.

6. DIELECTRIC HEATING EFFECT

Dielectric heating is caused by the absorption of electromagnetic energy in the dielectric medium through reorientation of the molecular dipoles. The absorption is especially strong when the frequency of the applied field is close to the frequency region of dielectric relaxation. The heating mechanism in isotropic dielectrics is well known, and the major application of the dielectric heating, namely, the microwave heating, is used for food processing. Dielectric heating effects in the NLCs are less useful since the induced temperature changes cause the change of the liquid crystal properties and thus affect the NLC switching behavior.

The first model of dielectric heating in NLC has been developed by Schadt [9]. In his model, the temperature decrease across the bounding (glass) plates of the NLC cell was considered negligibly small. The corresponding experiment on dielectric heating was performed for NLC cells of thickness 15 μm by placing a 80 μm thermocouple at one of the silver electrodes (apparently outside the cell) [9]. These studies were expanded in our previous work by using a much smaller thermocouple inserted directly into the NLC slab [8]. Recently, Wen and Wu proposed a new, noncontact, method [10] based on the measurements of phase retardation changes caused by the temperature-induced changes of the birefringence Δn of the NLC. This technique is applicable when the electric field causes no reorientation of the director (otherwise the phase retardation would change because of the director reorientation), i.e. when the following conditions are satisfied: (1) the material has a negative dielectric anisotropy, $\Delta\varepsilon(f) < 0$, (2) the cell yields a strict planar alignment (zero pretilt angle) and (3) the electric field causes no hydrodynamics. Because of these limitations, the technique cannot address the issue of dielectric heating in the region of dielectric relaxation for $\varepsilon_{\parallel}(f)$.

Below, we explore briefly the dielectric heating effects caused by the dielectric relaxation of $\varepsilon_{\parallel}(f)$ by expanding the theoretical model to include the finite thermal conductivity of the bounding plates; a more detailed investigation of dielectric heating effects is presented in [11]. Evidently, the temperature changes should depend not only on the electric field, properties of the NLC and bounding plates, but also on the thermal properties of the medium in which the NLC cell is placed; however, to the best of our knowledge, this issue has not been explored in the prior work. To directly measure the temperature of the nematic

slab in the broad range of field frequencies, one can use the direct method with a tiny thermocouple smaller than the cell thickness, as described in Refs. [8,11].

When a nematic cell is driven by a harmonic electric field $\mathbf{E}(t) = \mathbf{E}_0 \cos \omega t$, the dielectric heating power density P can be written as:

$$P = \frac{\omega \varepsilon_0 \mathbf{E}_0 \cdot \varepsilon^i(\omega) \cdot \mathbf{E}_0}{2}, \tag{7}$$

where ε^i is the imaginary part of the dielectric tensor ε. The dielectric tensor ε and thus the heating power density P depend on the orientation of the NLC director $\hat{\mathbf{n}}$. In what follows, for the sake of simplicity, we assume that the electric field is homogeneous inside the cell. This assumption is valid when the director field is uniform or only weakly distorted across the cell (including the case of a very strong voltage when most of the NLC is reoriented) or when the dielectric anisotropy of the LC material is weak. Therefore, we represent the electric field through the applied voltage U acting across a NLC cell of a thickness d, $\mathbf{E}_0 = U\hat{\mathbf{z}}/d$, so that

$$P = \frac{\pi f \varepsilon_0 \varepsilon^i_{zz} U^2}{d^2}, \tag{8}$$

where $\varepsilon^i_{zz} = \varepsilon^i_\perp \sin^2 \theta + \varepsilon^i_\parallel \cos^2 \theta$ is the imaginary part of the effective dielectric permittivity, and θ is the angle between $\hat{\mathbf{n}}$ and the normal $\hat{\mathbf{z}}$ to the bounding plates, as described in Eq. (23).

Let us discuss now the scheme of the dielectrically-induced heat production and its transfer in the multilayered system comprised of an NLC layer, two bounding plates of finite thickness (but of infinite size in the two other directions), placed into different surrounding media.

The heat conduction equation for each of the layers is of a generic form [12]

$$c_p \rho \frac{\partial T(z,t)}{\partial t} = G \frac{\partial^2 T(z,t)}{\partial z^2} + P_0, \tag{9}$$

where c_p is the heat capacity of the layer, ρ is the material density, G is the layer's thermal conductivity, P_0 is the specific heat production inside the layer. Equation (27) should be accompanied with the boundary conditions that guarantee the heat flow balance.

For the case of the NLC layer, $P_0 = P$. The temperature drop across the NLC slab is maximum for a stationary regime. For a stationary case, Eq. (9) (with the left hand side being zero) allows us to estimate the temperature drop as $\Delta T_{lc}(t) \leq Pd^2/8G = \pi f \varepsilon_0 \varepsilon^i_{zz} U^2/8G$. Consider a

typical situation, $G \sim 0.2\,\mathrm{W/mK}$ [13], $\varepsilon^i_{zz} \sim 1$, $U \sim 50\,\mathrm{V}$, $f \sim 10^6\,\mathrm{Hz}$, the temperature drop is less than the order of $0.05^\circ\mathrm{C}$. Therefore, we can assume that the temperature drop across the (relatively thin) NLC layer is small and concentrate on the temperature changes in the bounding plates. This small temperature difference in the NLC layer mitigates the possible measurement error caused by the finite size of the thermocouple which is comparable to the cell thickness.

In what follows, we consider the system being symmetric with respect to the middle plane of the NLC cell and apply Eq. (9) to describe the heat conduction through one of the two bounding plates, for example, the one located within $z \in [d/2, d/2+L]$ or $\tilde{z} \in [0, L]$, where $\tilde{z} = z - d/2$ is introduced to simplify the notations. Equation (27) needs to be supplemented by two boundary conditions for the heat transfer, at the NLC-bounding plate interface and at the bounding plate-surrounding medium interface. Because the NLC layer is thin as compared to the bounding plates, one can neglect the heat stored in the NLC layer itself, so that the heat flux from the NLC layer to the bounding plate is $Q_{\mathrm{in}} = Pd/2$. We assume that the heat flux Q_{out} at the bounding plate-surrounding medium interface obeys the Newton's cooling law, i.e., $Q_{\mathrm{out}} = k(T(\tilde{z} = L, t) - T_0)$, where $T(\tilde{z} = L, t)$ is the temperature of the plates outer boundary, T_0 is the temperature of the surrounding medium at infinity, and k is the heat transfer coefficient of the surrounding medium. The boundary conditions are then written as:

$$\frac{\partial T(\tilde{z}=0,t)}{\partial z} = -\frac{Pd}{2G}, \quad \frac{\partial T(\tilde{z}=L,t)}{\partial z} = -\frac{k}{G}\Big(T(\tilde{z}=L,t) - T_0\Big), \qquad (10)$$

where $T(\tilde{z}=0,t)$ is the temperature of the NLC-bounding plate interface. The solution $T(\tilde{z},t)$ of Eq. (9), supplemented with the boundary conditions in Eq. (10) and the initial condition $T(\tilde{z}=0,t) = T_0$, is

$$T(\tilde{z},t) = T_0 + \Delta\overline{T}_k\left[1 + \xi\left(-\frac{\tilde{z}}{L}+1\right) - \sum_{n=1}^{\infty} a_n \cos q_n \frac{\tilde{z}}{L}\exp\left(-\frac{t}{\tau_n}\right)\right], \quad (11)$$

where

$$\Delta\overline{T}_k = \frac{\pi f \varepsilon_0 \varepsilon^i_{zz} U^2}{2kd} \qquad (12)$$

is some characteristic temperature drop; as we shall see later, $\Delta\overline{T}_k$ is the stationary value of the temperature difference between the bounding plate's external boundary $\tilde{z} = L$ and the point $\tilde{z} \to \infty$ in the surrounding medium. The constant $\xi = kL/G$ is called the Biot number, $a_n = 2\tan q_n/(\sin q_n \cos q_n + q_n) > 0$ are the dimensionless

coefficients with the eigenvalues q_n satisfying the equation $q_n \tan q_n = \xi$, and $\tau_n = c_p \rho L^2 / G q_n^2$ are the characteristic time constants determining the transition to the stationary regime. For the convenience of further analysis, we will consider the temperature change $\Delta T(t)$ of NLC measured as the difference between the temperature of the NLC bulk and the temperature T_0 at infinity, $\tilde{z} \to \infty$ (which is also the initial temperature of the whole system),

$$\Delta T(t) = \Delta \overline{T}_k \left[1 + \xi - \sum_{n=1}^{\infty} a_n \exp\left(-\frac{t}{\tau_n} \right) \right], \tag{13}$$

as the sum of the following two contributions,

$$\Delta T(t) = \Delta T_k(t) + \Delta T_g(t), \tag{14}$$

where

$$\Delta T_k(t) = T(\tilde{z} = L, t) - T_0 = \Delta \overline{T}_k \left[1 - \sum_{n=1}^{\infty} a_n \cos q_n \exp\left(-\frac{t}{\tau_n} \right) \right] \tag{15}$$

is the difference between the temperature $T(\tilde{z} = L, t)$ of the bounding plate's external boundary, and T_0, and $\Delta T_g = T(\tilde{z} = 0, t) - T_0(\tilde{z} = L, t)$ is the temperature difference across the bounding (say, glass) plate, Figure 9.

As one can see from Eqs. (13)–(15), the stationary value $\Delta T_k(t \to \infty)$ is indeed equal to $\Delta \overline{T}_k$; besides, $\Delta T_g(t \to \infty) = \Delta \overline{T}_g = \xi \Delta \overline{T}_k$. Therefore, the temperature increase of the NLC slab, $\Delta \overline{T} = \Delta T(t \to \infty)$ can also be represented by the sum of two terms:

$$\Delta \overline{T} = \Delta \overline{T}_k (1 + \xi) = \frac{\pi f \varepsilon_0 \dot{\varepsilon}_{zz}^i U^2}{2kd} \left(1 + \frac{kL}{G} \right). \tag{16}$$

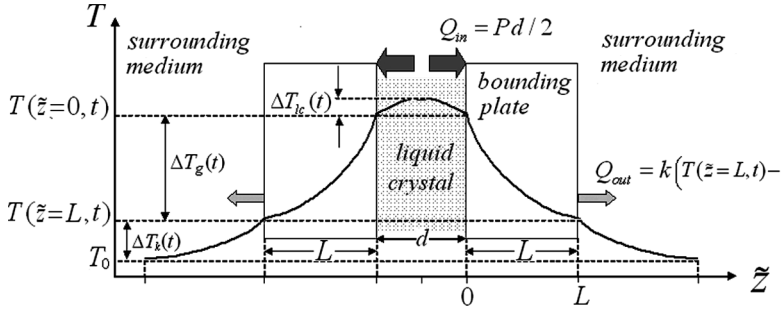

FIGURE 9 The scheme of the dielectric heating of an NLC cell.

The model above, Eqs. (13)–(16), suggests that one can distinguish two regimes of dielectric heating. When $\xi \gg 1$, the temperature increase of the NLC is controlled mainly by the temperature gradient in the bounding (glass) plates. For $\xi \ll 1$, the dominating control parameter is the heat transfer coefficient k of the surrounding medium, $\Delta T(t) \approx \Delta T_k(t)$. Note that in the second case, the model above and the Schadt's model [9] predict different dynamics of the temperature increase.

Equation (16) indicates that the NLC temperature change is influenced by many factors, including the liquid crystal's imaginary dielectric permittivity component ε''_{zz}, the electric field (voltage U and frequency f), the thermal properties of the surrounding medium (heat transfer coefficient k), and the properties of the bounding plates (thermal conductivity G, heat capacity c_p, thickness L). It would be of interest to verify all the dependencies experimentally, especially the new effects of the temperature changes on the director reorientation and vice versa. Such a work is in progress.

To examine how the heat transfer coefficient k of the surrounding media affects the dielectric heating-induced temperature raise of the nematic cell, we used the following line of the surrounding media, in which k is expected to decrease: (1) aluminum cooling devices, (2) circulating air, (3) still air, and (4) Styrofoam.

Figure 10 illustrates the temperature dynamics caused by the dielectric heating effect for the NLC cell placed in four different surrounding media. The applied electric field ($U = 25\,\mathrm{V}$, $f = 500\,\mathrm{kHz}$) causes no director reorientation from the planar state. The temperature change is different in different media. First, the temperature change shows a tendency of saturation in media with good heat transfer (relatively high k), namely, with circulating air and aluminum surroundings. The temperature increase is small for the cooled aluminum surrounding and then increases in circulating and still air, which is a naturally expected result. For Styrofoam with poor heat transfer, the temperature increase is the largest and is not showing clear signs of saturation, at least within the time of the experiment, Figure 10.

Theoretically, Eq. (15), the NLC temperature increase $\Delta T(t)$ depends on series, $a_n \exp(-t/\tau_n)$. The first term $n = 1$ in this series is dominant, because of the two reasons. First, the characteristic times $\tau_n = c_p \rho L^2 / G q_n^2$ with $n > 1$ are at least 9 times smaller than τ_1 and shorter than 0.3 s. By using $c_p = 840\,\mathrm{J/kgK}$ [14], $\rho = 2.44 \times 10^3\,\mathrm{kg/m^3}$ [15,16], $G = 0.94\,\mathrm{W/mK}$ [16], one finds $\tau_n = 2.6/q_n^2$ s; since $q_n > (n-1)\pi$, the largest relaxation time with $n > 1$ is thus $\tau_2 < 0.3$ s. Second, the first amplitude a_1 is at least 6 times larger than

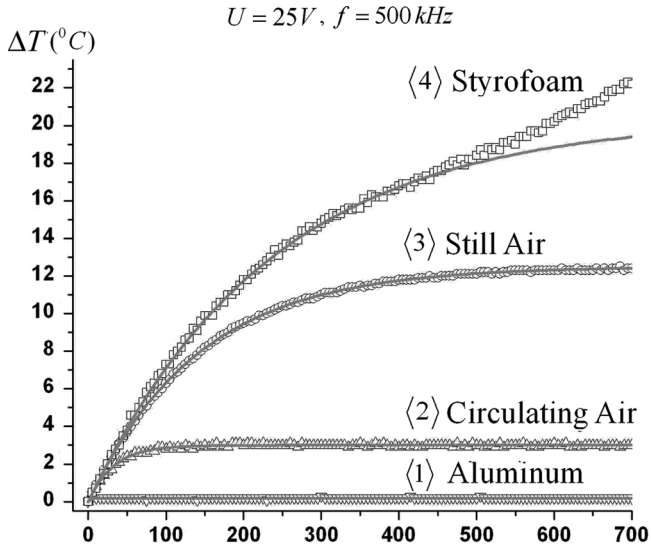

FIGURE 10 Temperature dynamics of a DFN MLC2048 cell surrounded by different media (1) aluminum cooling devices, (2) circulating air, (3) still air, and (4). The initial temperature is 23°C. The applied voltage is 25 V and 500 kHz. The error bars are smaller than the size of the data points. The solid lines are theoretical fits, Eq. (17).

the sum of the amplitudes of all other terms. Equation (15) is then simplified,

$$\Delta T(t) = \Delta \overline{T}\left[1 - \exp\left(-\frac{t}{\tau_1}\right)\right], \tag{17}$$

where

$$\tau_1 = \frac{c_p \rho L^2}{G q_1^2}. \tag{18}$$

Equation (17) describes the experimentally observed temperature dynamics for aluminum and air surrounding rather well, Figure 10; it fits the experimental data with $\Delta\overline{T} = 0.2$°C, $\tau_1 = 1.3$ s (1), $\Delta\overline{T} = 3.0$°C, $\tau_1 = 32.2$ s (2), and $\Delta\overline{T} = 12.5$°C, $\tau_1 = 141.8$ s (3). However, Eq. (17) does not describe the Styrofoam experiment (4): The departures are most naturally related to the fact that the Newton law (used in the model) is not justified when the surrounding medium has poor heat transfer efficiency.

The data presented in Figure 10 allow us to determine the heat transfer coefficients k from the fitted values of τ_1 and $\Delta\overline{T}$. We first determine $q_1 = L\sqrt{c_p\rho/G\tau_1}$ and then find k from the equation $q_1 \tan q_1 = kL/G$. For the aluminum cooling device, $k = 8267\,\mathrm{W/m^2K}$; for circulating air, $k = 72\,\mathrm{W/m^2K}$; and for still air, $k = 16\,\mathrm{W/m^2K}$. The data for air are in the expected range of 10–100 $\mathrm{W/m^2\,K}$. Moreover, by substituting the found values of k into Eq. (16) and using the experimentally measured $\Delta\overline{T}$, we find that the quantity $\varepsilon''_{zz} \approx 1.8$ is the same for all three experiments with different media (1), (2) and (3), as it should be, as ε''_{zz} is the NLC material parameter (the imaginary part of the dielectric tensor component). The same value of ε''_{zz} was measured independently by using the impedance analyzer SI-1260 (Schlumberger Inc.), which testifies that the theoretical model describes the experimental data rather well.

7. CONCLUSION

We propose a general model to quantitatively describe the orientation dynamics of dispersive liquid crystals in which the assumption of the instantaneous relationship between the electric displacement and the electric field is lifted. This time scale is typically in the sub-millisecond range which is of great interest for modern fast-switching devices. The proposed model expresses the electric displacement $\mathbf{D}(t)$ as the function of the static dielectric properties of the NLC, the present and past electric field and the present and past director. Recently, we generalized the description of dielectric memory effect [17], by lifting the restriction of a single relaxation process and considering multiple relaxations that might occur in both $\varepsilon_{\|}$ and $\varepsilon_{\perp}$. The proposed model should be also applicable to dynamic reorientation of other LC phases; in the case of ferroelectric LCs, the theory should be supplemented by the consideration of spontaneous electric polarization. We demonstrated that the phenomenon of dielectric dispersion, slow relaxation and dielectric heating should be taken into account in the development of fast-switching LC devices. The electric field alone, through the balance of two different mechanisms of anisotropic coupling between electric field and LC, namely, director reorientation and anisotropic dielectric heating, can create the thermodielectric bistability [18]. This bistability might be of practical importance, because of (a) the optical contrast between the two states is extremely sharp and (b) the states can be switched between with a very low power. The next step is to use the theory outlined above in the optimization of the driving voltage pulses to achieve the fastest possible response times.

REFERENCES

[1] Takanashi, H., Maclennan, J. E., & Clark, N. A. (1998). *Jpn. J. Appl. Phys*, *37*, 2587.
[2] Golovin, A. B., Shiyanovskii, S. V., & Lavrentovich, O. D. (2003). *Appl. Phys. Lett.*, *83*, 3864.
[3] Frohlich, H. (1958). *Theory of Dielectrics*, 2nd ed. Oxford: London.
[4] Yin, Y., Shiyanovskii, S. V., Golovin, A. B., & Lavrentovich, O. D. (2005). *Phys. Rev. Lett.*, *95*, 087801.
[5] Schadt, M. (1997). *Annu. Rev. Mater. Sci.*, *27*, 305.
[6] Haase, W. & Wrobel, S. (2003). *Relaxation Phenomenon*, Springer: New York.
[7] Bottcher, C. J. F. & Bordewijk, P. (1978). *Theory of Electric Polarization*, Elsevier: New York, Vol. 2.
[8] Yin, Y., Gu, M., Golovin, A. B., Shiyanovskii, S. V., & Lavrentovich, O. D. (2004). *Mol. Cryst. Liq. Cryst.*, *421*, 133.
[9] Schadt, M. (1981). *Mol. Cryst. Liq. Cryst.*, *66*, 319.
[10] Wen, C. H. & Wu, S. T. (2005). *Appl. Phys. Lett.*, *86*, 231104.
[11] Yin, Y., Shiyanovskii, S. V., & Lavrentovich, O. D. (2006). *J. Appl. Phys.*, *100*, 024906.
[12] Fourier, J. (1955). *The Analytical Theory of Heat*, Dover: New York.
[13] Ahlers, G., Cannell, D. S., Berge, L. I., & Sakurai, S. (1994). *Phys. Rev. E*, *49*, 545.
[14] Muneer, T., Kubie, J., & Grassie, T. (2003). *Heat Transfer: A Problem Solving Approach*, Taylor & Francis: New York.
[15] Chawla, K. K. (2003). *Composite Materials*, 2nd ed. Krishan Kumar: Norwell, MA.
[16] http://www.valleydesign.com/sodalime.htm.
[17] Gu, M., Yin, Y., Shiyanovskii, S. V., & Lavrentovich, O. D. (2007). *Phys. Rev. E*, *76*, 061702.
[18] Yin, Y., Shiyanovskii, S. V., & Lavrentovich, O. D. (2007). *Phys. Rev. Lett.*, *98*, 097801.